Experimental investigation on combustion and emission characteristics of non-premixed ammonia/hydrogen flame

Zhang, Fangyu; Zhang, Gengxin; Wang, Zhongcheng; Wu, Dawei; Jangi, Mehdi; Xu, Hongming

DOI:
10.1016/j.ijhydene.2024.02.281

Document Version
Publisher's PDF, also known as Version of record

Citation for published version (Harvard):
Zhang, F, Zhang, G, Wang, Z, Wu, D, Jangi, M & Xu, H 2024, 'Experimental investigation on combustion and emission characteristics of non-premixed ammonia/hydrogen flame', *International Journal of Hydrogen Energy*, vol. 61, pp. 25-38. https://doi.org/10.1016/j.ijhydene.2024.02.281

International Journal of Hydrogen Energy 61 (2024) 25–38

Contents lists available at ScienceDirect

International Journal of Hydrogen Energy

journal homepage: www.elsevier.com/locate/he

Experimental investigation on combustion and emission characteristics of non-premixed ammonia/hydrogen flame

Fangyu Zhang [a], Gengxin Zhang [a], Zhongcheng Wang [b], Dawei Wu [a,*], Mehdi Jangi [a], Hongming Xu [a]

[a] Department of Mechanical Engineering, School of Engineering, University of Birmingham, Edgbaston, Birmingham, B15 2TT, UK
[b] Merchant Marine College, Shanghai Maritime University, Shanghai, 201306, China

ARTICLE INFO

Handling editor: J Ortiz

Keywords:
Ammonia-hydrogen combustion
Non-premixed flame
Flame stability
Emissions
Chemiluminescence

ABSTRACT

The use of ammonia and hydrogen as fuels to decarbonise the heavy transport industry has attracted worldwide attention. In this work, a swirl-enhanced combustion test rig has been built to investigate the combustion and emission characteristics of non-premixed ammonia/hydrogen flames. The blowoff limits were first examined to ensure that a range of stable flames could be achieved. Emissions containing nitric oxide (NO), nitrous oxide (NO_2), ammonia slip (NH_3) and unburnt hydrogen (H_2) were then measured with a variety of global equivalence ratios, hydrogen blending ratios, inlet gas temperature, swirl numbers and combustion chamber insulation conditions. The structure of non-premixed ammonia/hydrogen flames and the relationship between excited hydroxyl radicals (OH^*) and NO emission were revealed using OH^* chemiluminescence profiles. The stable non-premixed ammonia/hydrogen flames were achieved when the hydrogen blending ratio was greater than 20%. The optimal emission performance was achieved under stoichiometric conditions, as determined by combustion efficiency. The insulation conditions of the combustor wall played a key role in the emission results, as significant growth of NO and NO_2 as well as a reduction of ammonia slip were found. Although a lower swirl number improved the flame stability range, the increases in NO and NO_2 emissions were observed.

1. Introduction

Electric vehicles introduce a new trend on the market of passenger cars and light-duty vehicles. However, the hard-to-decarbonise heavy transport sectors would not be possible to be solely driven by batteries due to their application backgrounds, such as heavy load and long distance. To decarbonise heavy transports, ammonia and hydrogen are considered as promising alternative fuels. Ammonia and hydrogen are both carbon-free, which avoids carbon emissions during the combustion of ammonia and hydrogen. As ammonia has been extensively applied as fertilizer and cleaning chemicals in agriculture, the production, storage and distribution processes of ammonia have been well established. Although the dominate way of producing ammonia in the current stage still relies on the conventional Haber-Bosch method, many projects on green ammonia production are ongoing [1–4]. If the production of green ammonia can be commercially introduced, the carbon footprint in the life cycle is expected to be significantly reduced. Owning to the physical properties similarity as propane, it is easy for ammonia to be stored as liquified ammonia under approximately $-34\ ^{\circ}C$ at atmospheric pressure and compressed ammonia in an around 10 bar tank at room temperature. Given these advantages, ammonia, as one of the highly competitive hydrogen carriers, is worthy of in-depth research and discussion as a green alternative fuel.

Nevertheless, the direct adoption of ammonia as a fuel has encountered challenges. The narrow flammability (around $18\% - 28\%$ fuel mole fraction) [5], the high ignition temperature ($903\ K$) [6] and the low laminar flame speed ($\sim 0.07 m/s$ @NTP (normal temperature and pressure)) [7–9] of ammonia make it difficult to be ignited and maintain robust flame. Due to the high reactivity and high laminar flame speed of hydrogen, it is considered to be an ideal enhancer for ammonia flames [10–14]. Joo et al. [10] studied the flame stability of premixed ammonia/hydrogen flames in a tube type combustor at NTP. The findings concluded the stability limits increased as more hydrogen was blended with ammonia. The comparison of combustion limits between premixed ammonia/hydrogen flames and premixed ammonia/methane flames was conducted experimentally [11]. It was concluded that hydrogen

* Corresponding author.
E-mail address: d.wu.1@bham.ac.uk (D. Wu).

https://doi.org/10.1016/j.ijhydene.2024.02.281
Received 7 November 2023; Received in revised form 9 January 2024; Accepted 21 February 2024
Available online 28 February 2024

addition showed a wider combustion limit than methane addition into premixed ammonia flames. Furthermore, elevating the inlet temperature had a great impact on expanding the combustion limits of premixed ammonia/hydrogen flames and premixed ammonia/methane flames. Wei et al. [15] analysed the lean blowoff characteristics of premixed ammonia/hydrogen combustion in a gas turbine combustor. The flame structure and flow field results showed that there were less large-scale and more small-scale wrinkles in the flame front when 10% hydrogen was premixed with 90% ammonia. The promoted combustion intensity facilitated the flame stability. A generic swirl burner was used to test the stability limits of premixed ammonia/hydrogen flames up to 5 *bar* in KAUST (King Abdullah University of Science and Technology) [12]. It indicated that the stability range was broadened by increasing the pressure, however, the impact was inapparent. Moreover, the results showed that 40% NH_3/ 60% H_2 flame was surprisingly stabilised even at very lean conditions (the equivalence ratio was at approximately 0.3). Zhen et al. [16] studied the flame stability of premixed ammonia/hydrogen Bunsen flames for impingement heating applications. It was found that there exists a critical value of hydrogen addition to obtain a stable premixed ammonia/hydrogen Bunsen flame for a given Reynolds number of the fuel/air mixture jet and equivalence ratio. It is evident that a majority of scholars have initiated research on the combustion characteristics of premixed ammonia and hydrogen, however, there are few studies on the flame stability limits of non-premixed ammonia/hydrogen flames so far.

Emissions are another concern in the combustion of ammonia and hydrogen. While carbon emissions are effectively reduced, high-temperature conditions, particularly when ammonia with nitrogen atoms is present, can lead to fuel-bound *NO* formation. Valera-Medina et al. [17] carried out a 50% NH_3/ 50% H_2 premixed flame under fuel-lean conditions ($\varphi: 0.41-0.56$) in Gas Turbine Research Centre (GTRC) in Cardiff University under NTP. The NO_x emission was high in fuel-lean conditions and reached over 1000 *ppmv* when the equivalence ratio was 0.52 and 0.56. Later, the same research group [18] investigated premixed 70% NH_3/ 30% H_2 and 60% NH_3/ 40% H_2 combustion under fuel-rich conditions, but it was noticed that 60% NH_3/ 40% H_2 flame tended to flashback. It was observed that the NO_x emission decreased when the equivalence ratio increased from 1.0 to 1.4. Experimental results of ammonia slip were not published in this work though. *NO* emission from premixed ammonia flames and premixed ammonia/hydrogen flames was investigated in a porous combustor by Chen et al. [19]. When the equivalence ratio increased from 1.0 to 1.2, *NO* emission decreased by 98.3% to 23.6 *ppm*. The calculated conversion rate of nitrogen atoms in the fuel to *NO* was very low under fuel-rich conditions for both premixed ammonia flames and premixed ammonia/hydrogen flames. Compared to pure ammonia combustion, the conversion rate of *NO* was only 0.42% higher when 30% hydrogen was added to the fuel. Recently, Tong et al. [20] analysed premixed ammonia/hydrogen/oxygen combustion by building a 3D meso-scale combustor model. The model was employed to investigate the *NO* emissions under different hydrogen additions ($0-20\%$). The results presented that increasing hydrogen addition to 15% resulted in *NO* emission reduction at a given low inlet velocity (less than $0.4\,m/\,s$) under stoichiometric conditions. However, as the hydrogen addition increased to 20%, *NO* emission was increased. The relationship between *NO* concentration and OH^* in premixed ammonia/hydrogen flames was explored under fuel-lean conditions by Zhu et al. [21]. The local *NO* concentration and *NO* emission were found to align well with the local OH^* chemiluminescence intensity in the combustor when the equivalence ratio was at $0.40-0.85$ and ammonia concentration in the fuel was greater than 0.25. It indicates OH^* chemiluminescence imaging technology can be employed to qualitatively visualise local *NO* concentration trends or *NO* emission trend in premixed ammonia/hydrogen flames which is a very cost-effective approach compared to local *NO* detection using *OH*-PLIF technology. Pugh et al. [22] investigated OH^*, NH_2^*, NH^* chemiluminescence in premixed and non-premixed ammonia/air flame as well as partially premixed 70% NH_3/ 30% H_2 flame with the same net thermal power at 25 *kW*. There were two types of configurations of partially premixed ammonia/hydrogen flame. One is premixed ammonia and air entering from outer swirling flow and hydrogen entering from the central flow, which was called H_{2Diff}. The other is premixed hydrogen and air entering from outer swirling flow and ammonia entering from the central flow, which is called NH_{3Diff}. By comparing the premixed ammonia flame, H_{2Diff} and NH_{3Diff}, it was noted that for the case of NH_{3Diff}, NH_2^* chemiluminescence intensity was the greatest and OH^* and NH^* chemiluminescence intensities were the lowest among three. Meanwhile, *NO* emission produced in NH_{3Diff} showed the lowest value. When both the temperature and pressure were lifted, a similar relational phenomenon was observed, i.e., NH_2^* intensity increased, OH^* intensity and *NO* emission decreased. Moreover, a significant reduction of *NO* was observed in non-premixed ammonia/air flame compared to premixed ammonia/air flame, with 200 *ppmvd*@15% O_2 under stoichiometric condition, but with a high ammonia slip. Nonetheless, it is still unclear about the emission characteristics of non-premixed ammonia/hydrogen flames, especially with different hydrogen blending ratios and swirlers. Experimental data on NO_x emission has been reported in many studies, but it is equally important to have unburnt ammonia and hydrogen to provide solid evidence for chemical mechanism development and model validation.

It is essential to conduct a thorough investigation on the combustion and emission characteristics of non-premixed ammonia/hydrogen flames in a swirl-enhanced combustor. To the best of our knowledge, this area has not been extensively explored. In this paper, the stable range conditions of non-premixed ammonia/hydrogen flame were first identified by measuring the blowoff limits. Secondly, emissions including NO_x and unburnt ammonia and hydrogen at the exhaust were analysed with various global equivalence ratios, hydrogen blending ratios, inlet gas temperature, combustor wall conditions and swirl numbers. OH^* chemiluminescence images were then used to reveal the flame structure. For the quantitative analysis, OH^* intensity was calculated based on pixel data of the OH^* chemiluminescence images. The experimental results are anticipated to make a significant contribution to the validation of computational fluid dynamics models and to the development of ammonia combustion mechanisms. In turn, it provides guidance for the development of ammonia/hydrogen fuelled heat engines for use in the heavy transport sectors.

2. Methodology

2.1. Experimental test rig

All the experiments were conducted in the Future Engines & Fuels Laboratory at the University of Birmingham. The non-premixed combustion chamber is cylindrical with a detachable quartz glass window. The inner diameter of the combustion chamber is 150 *mm* with 310 *mm* in length. The optical window is in rectangular shape ($249\,mm \times 53\,mm$). Fuel blend enters the combustion chamber through an 8-hole fuel nozzle while air enters through a swirler on the annulus of the fuel nozzle. The injection angle of the fuel nozzle is determined to be 45° in the present work as it was concluded by Okafor et al. [23] that 45° shows the best performance of mixing fuel and air near the inlet in ammonia combustor among four different injection angles ($0°, 30°, 45°, 60°$). Swirl-enhanced strategy is utilised for air injection to promote the ammonia flame robustness. Fig. 1 demonstrates the swirler diagram with a vane angle, α. There are three different swirlers available for investigation with the vane angle at $40°, 45°, 50°$. The technical data of the swirlers is illustrated in Table 1. Swirl number (S) is used to represent the strength of the swirling flow. It is determined as the ratio of the axial flux of angular momentum to the axial flux of the axial momentum [24]. The swirl number is calculated using the equation [25]:

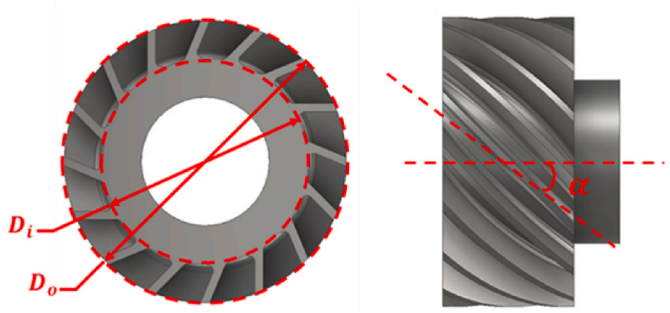

Fig. 1. Swirler.

Table 1
Swirler details.

Swirler	α (°)	D_i (mm)	D_o (mm)	Number of vanes (−)	S (−)
S(a)	40	32	44	16	0.73
S(b)	45	32	44	16	0.87
S(c)	50	32	44	16	1.04

$$S = \frac{2}{3} \bullet \frac{1 - \left(\frac{D_i}{D_o}\right)^3}{1 - \left(\frac{D_i}{D_o}\right)^2} \bullet tan\ \alpha \tag{1}$$

where D_i, D_o and α represent the inner diameter, the outer diameter of the swirler and the vane angle, respectively. In the present work, swirl number is changing between 0.73, 0.87 and 1.04, which is sufficient (above 0.6) to obtain a strong swirling flow [26–28].

Fig. 2 illustrates the schematic diagram of experiment test rig, which spans two test rooms and two control rooms. It is comprised primarily of gas cylinders, air compressor, mass flow controllers (MFCs) for each gas, flame arrestors, flame mixer, in-line heating pipes with their temperature controllers, combustion chamber, thermocouples, purge system, high speed COMS camera, heated sample lines, an emission multi-gas analyser for NO_x and O_2 measurements, a gas chromatography for NH_3 and H_2 measurements, a data acquisition device and a computer.

Ammonia (99.98% purity) and hydrogen (99.99% purity) were supplied in pressurised gas cylinders from BOC company. The flow rate of ammonia and air were controlled by Aalborg™ MFC model GFC57S-BDN2 and GFC67S-VEN2, respectively, with the accuracy at ±3.0% of set point for 0 − 20% of full-scale range scale and ±1.5% of set point for 20 − 100% of full-scale flow. The MFC for hydrogen is model GFC47S-VDN6 with the accuracy within ±1.0% of set point for full-scale flow. The ignition system is composed of a power supply, capacitor discharge ignition, a pulse generator, an ignition coil and two electrodes. Two electrodes are made of stainless steel with sharpened tip at the front. The negative electrode is mounted on the inlet plate of the combustor. The positive electrode is inserted from the bottom plate of the combustor. The electrodes gap is approximately 3 *mm*.

The total input thermal power (P) was maintained at 8 *kW* throughout the test cases. The mass flow rate of fuel blends ($\dot{m}_{fuel}$) was calculated based on the total input thermal power and LHVs (Lower Heating Values) of the individual fuels using the equation as follows:

$$\dot{m}_{fuel} = \frac{P}{LHV_{NH_3} \times x[NH_3] + LHV_{H_2} \times x[H_2]} \tag{2}$$

where LHV_{NH_3}, LHV_{H_2} denote the LHVs of ammonia and hydrogen, which is 18.8 MJ/kg and 120 MJ/kg, respectively; $x[NH_3]$ and $x[H_2]$ represent the mole fraction of ammonia and hydrogen in the fuel blend. Hydrogen blending ratio ($x\%\ H_2$) is calculated by dividing the concentration of hydrogen in the total fuel blend, shown as:

$$x\%\ H_2 = \frac{x[H_2]}{x[H_2] + x[NH_3]} \tag{3}$$

The global equivalence ratio (φ_{global}) is the ratio of the fuel-air ratio to the stoichiometric fuel-air ratio using the equation below and controlled by adjusting the mass flow rates of the fuel blend and air:

$$\varphi_{global} = \frac{\dot{m}_{fuel}/\dot{m}_{air}}{(\dot{m}_{fuel}/\dot{m}_{air})_{st}} \tag{4}$$

where $\dot{m}_{fuel}$ and $\dot{m}_{air}$ represents the mass flow rate of fuel and air respectively; $(\dot{m}_{fuel}/\dot{m}_{air})_{st}$ represents the fuel-air ratio under the stoichiometric condition.

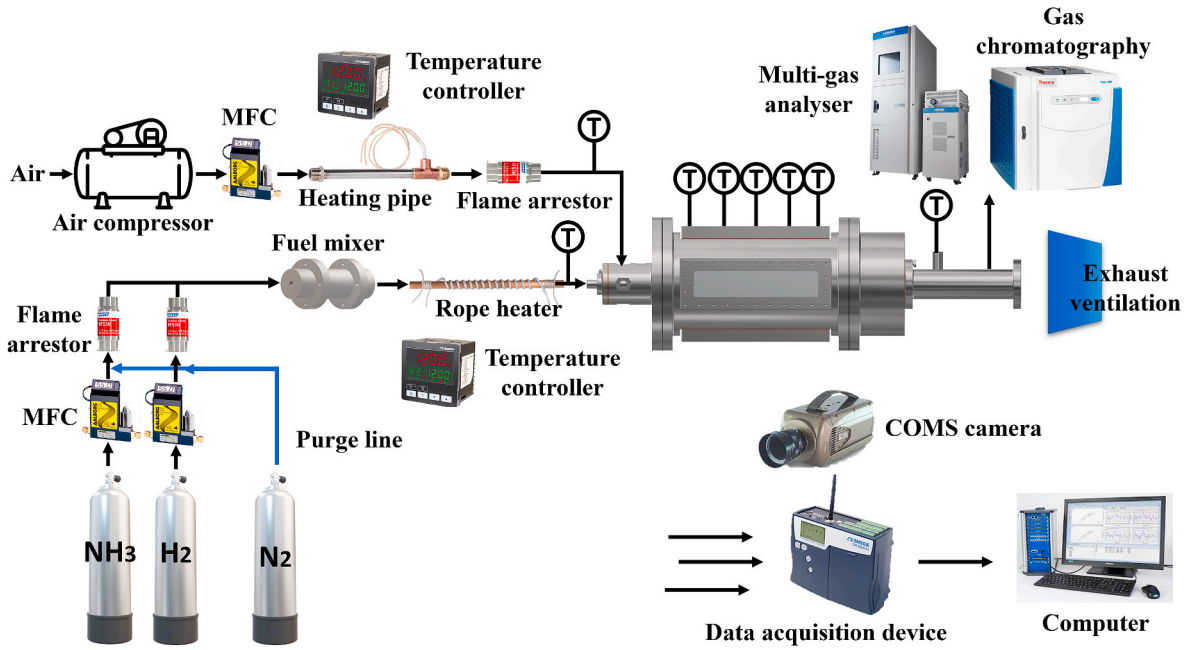

Fig. 2. Experiment test rig diagram.

2.2. Blowoff limits measurement

The blowoff limit is a critical parameter to ensure the range of a reliable flame. It is identified by gradually increasing the air flow rate by approximately 2% every 20 seconds while keeping the fuel flow rate unchanged until the flame is no longer sustained [29]. The global equivalence ratio at the blowoff limit is therefore calculated based on the measured air flow rate when the flame becomes stable and when the flame blows off. The blowoff limit of ammonia and hydrogen was investigated at different hydrogen blending ratios, inlet temperatures and swirl numbers so as to first gain the knowledge of the conditions of non-premixed ammonia/hydrogen flame stability. This would aid in the subsequent analysis on emission characteristics and OH^* chemiluminescence. The experimental conditions for examining the flame stability are shown in Table 2.

2.3. Emission measurement

Horiba multi-gas analyser (MEXA-7100DEGR) was performed to measure NO and NO_2 emissions and oxygen at the exhaust. The repeatability is within ±0.5% of the full scale for zero point or within ± 0.5% of the readings for span point. Thermo Fisher Trace 1300 gas chromatography with Pulse Discharge helium ionisation Detector (PDD) and Thermal Conductivity Detector (TCD) was utilised to obtain the concentration of unburnt ammonia and hydrogen at the exhaust. For both types of detectors, the repeatability of typical retention time is less than 0.0008 min and the repeatability of the typical peak area is less than 0.5% relative standard deviation. The sample gas was collected from the centreline of the exhaust duct through a heating pipe. The temperature of the gas in the heated sample pipe was kept at 193 $°C$ for Horiba multi-gas analyser and 140$°C$ for gas chromatography to prevent the water condensation and aqueous dissolution of ammonia. The heated sample pipe was coated with functionalised hydrogenated amorphous silicon to avoid adsorption of ammonia and deliver a faster response in the measurement. The NO_x emissions from non-premixed ammonia/methane using the current test rig were validated with the single-staged results of premixed ammonia/methane flames in the literature [30]. The trends of NO and NO_2 showed satisfactory agreements with the literature results. The effects of global equivalence ratios, hydrogen blending ratios, inlet temperature, swirl numbers and combustion chamber wall conditions on emissions of non-premixed ammonia/hydrogen combustion were conducted in the swirl-enhanced combustor. The experimental conditions are elaborated in Table 3. All data were collected while emission levels remained stable. As ammonia and hydrogen were burnt under different global equivalence ratios, oxygen normalisation was applied to compare the emissions fairly. According to the regulation in the UK [31,32], all the emission results were normalised to the standard oxygen concentration basis at 15% using the equation:

$$ppm_{norm} = ppm_{mea}\left[\frac{20.95 - 15}{20.95 - O_{2mea}}\right] \tag{5}$$

where ppm_{norm} and ppm_{mea} indicate the normalised emission concentration and measured emission concentration, respectively; O_{2mea} indicate the measured oxygen concentration in the exhaust gases [31].

The error bar was calculated using the standard deviation equation based on the five measurements:

$$\sigma = \sqrt{\frac{1}{5}\sum_{i=1}^{5}(x_i - \bar{x})^2} \tag{6}$$

where x_i and $\bar{x}$ represent the average value for each measurement and average value of the five times measurements, respectively. It indicates the uncertainty of the emission measurement at each point.

Table 2
The experimental conditions for blowoff limit test.

Factor	Range
Air flow rate	$1.37 - 6.87\ g/s$
Hydrogen blending ratio	20%, 30%, 40%
Fuel inlet temperature	$300, 400, 475\ K$
Air inlet temperature	$300, 400, 435\ K$
Swirl number	0.73, 0.87, 1.04

Table 3
Experimental conditions for emission measurements/OH^* chemiluminescence imaging.

Factor	Range
Global equivalence ratio	$0.6 - 1.2$
Hydrogen blending ratio	20%, 30%, 40%
Fuel inlet temperature	$300, 325, 350, 400\ K$
Air inlet temperature	$300, 325, 350\ K$
Swirl number	0.73, 0.87, 1.04
Combustion chamber wall condition[a]	with and without silicate ceramic fibre blanket insulation

[a] OH^* chemiluminescence imaging was performed without silicate ceramic fibre blanket insulation.

2.4. OH^* chemiluminescence imaging measurement and image post-processing

The use of chemiluminescence imaging for investigating radicals of interest is non-invasive, cost-effective and has been applied to a variety of combustion applications with small optical access [33–36]. Fig. 3 demonstrates the optical system for capture OH^* chemiluminescence images. A high-speed Phantom® v710 CMOS camera was utilised with resolution of 1280 × 800, sample rate at 100 pps and exposure time at 9900 μs. Hamamatsu Photonics C10880 image intensifier was fitted on the CMOS camera through the relay lens to intensify the chemiluminescence at low-light level and facilitate the image visualisation. The image intensifier gain was constant at 999 in all the measurements. As the OH^* chemiluminescence primarily occurs in the wavelength between 280 − 350 nm [37], UV lens (UV-Nikkor 105 mm f/4.5 lens) and narrowband filter (centre: 310 nm) are employed. In the present work, OH^* chemiluminescence images have been measured and post-processed in relation to the global equivalence ratios, hydrogen blending ratios, inlet temperatures and swirl numbers. Table 3 also reveals the experimental conditions for OH^* chemiluminescence imaging measurement.

For each case, a thousand images were collected and post-processed with the in-house developed MATLAB code. The raw chemiluminescence images were averaged and then background corrected with averaged background images. Minimum value correction and 2D 3 × 3 median filter were applied to remove noise. Since the images collected in the laboratory were line-of-sight and the combustion chamber provided equidistant boundary for the flames with the axisymmetric fuel nozzle and swirler, the Abel inversion algorithm [38, 39] was implemented to obtain a representative spatially resolved image of the OH^* chemiluminescence distribution assuming that the flames were axisymmetric. Namely, the Abel inversion algorithm was utilised to deconvolute each row of images into integrals using an expansion of cosine functions on the principle of Fourier analysis [38,39]. Considering the computation time, the expansion value of cosine functions was assigned to five in the present study. The processed time-averaged spatially resolved OH^* chemiluminescence images were presented with false colour mapping, as shown in Fig. 4(b). To quantify the OH^* chemiluminescence, OH^* intensity ($\mathrm{II}'_{\mathrm{OH}^*}$) was determined on a pixel-by-pixel basis in the image before the application of the Abel inversion algorithm using the formula as follows [40]:

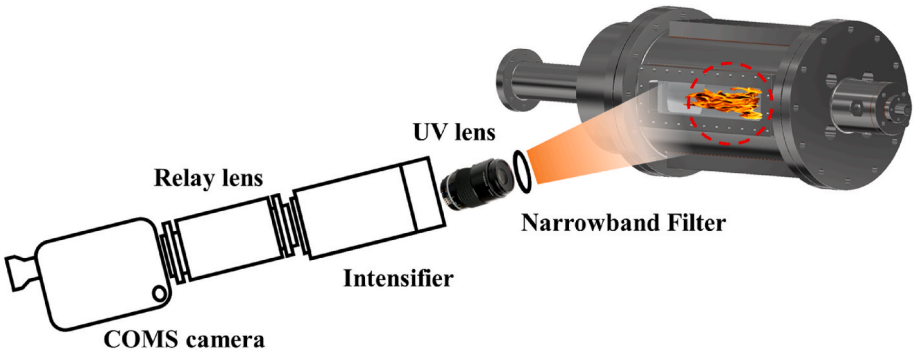

Fig. 3. Chemiluminescence visualisation setup.

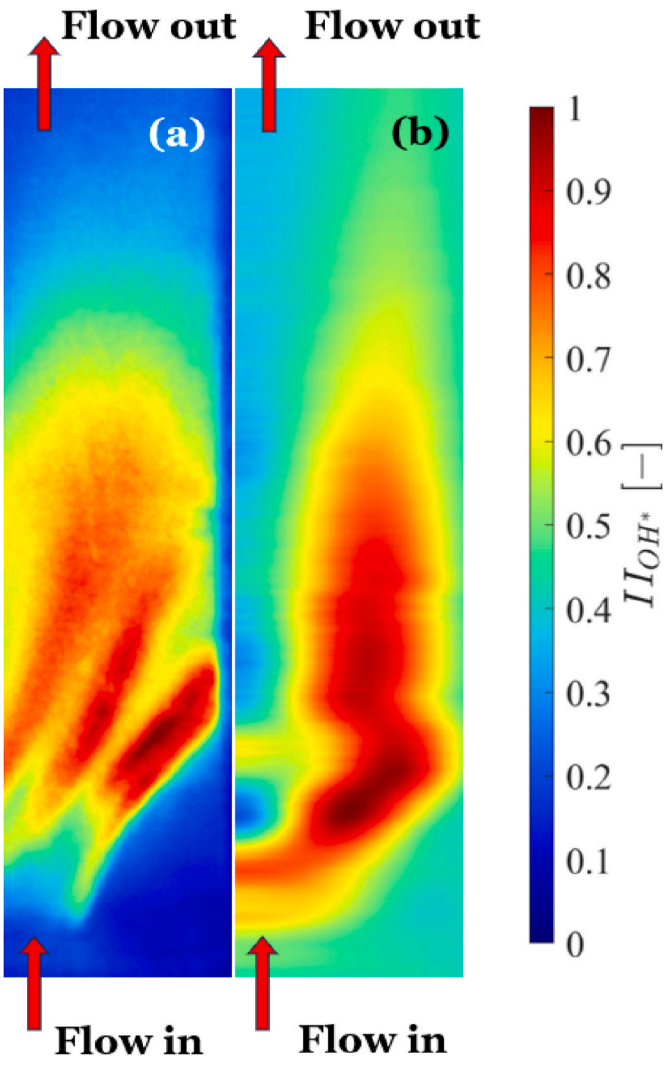

Fig. 4. Time-averaged OH^* chemiluminescence distributions (a) before and (b) after Abel inversion algorithm.

$$II'_{OH^*} = \sum_{i=1}^{800} \sum_{j=1}^{1280} \bar{I}_{OH^*_{ij}} \tag{6}$$

3. Results and discussion

3.1. Blowoff limits

It has been reported that ammonia flames have narrow flammability and low flame velocity, so it is important to determine the flame stability conditions when ammonia is used as the primary fuel and blended with a high flame velocity substance, hydrogen. Blowoff limits were examined with various hydrogen blending ratios and different swirlers at different gas inlet temperatures to ensure the flame stability condition and range (from lean blowoff limit to rich blowoff limit). The rich blowoff limit is defined as the minimum mass flow rate of air that can ignite and burn the fuel blends stably while the lean blowoff limit is defined as the maximum mass flow rate of air that keeps the flame stable before blowing away at a constant mass flow rate of fuel blends [41].

The effect of hydrogen blending ratios varying from 10% to 40% on the blowoff limits of non-premixed ammonia flames was conducted with swirler $S(b)$ (swirl number: 0.87) at the inlet gas temperature of 300 K. It is observed that the flame was not stabilised when only 10% hydrogen is blended with ammonia. When the hydrogen blending ratio is above 20%, the flame became stable. The rich and lean blowoff limits of non-premixed ammonia flames with 20%, 30%, 40% hydrogen addition is

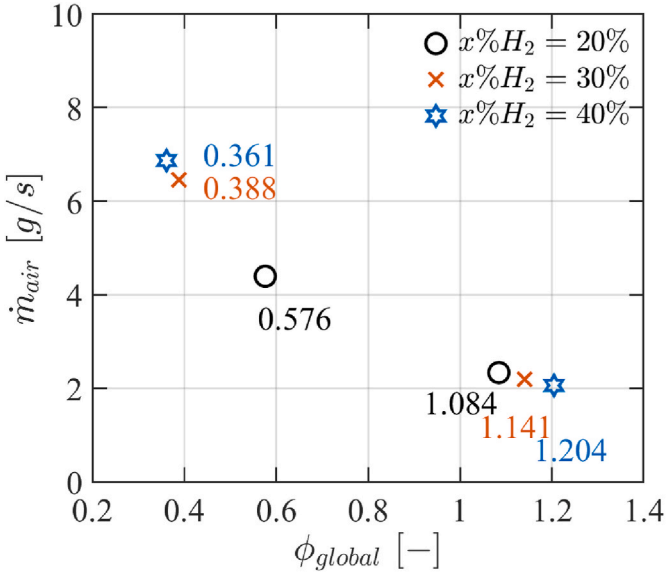

Fig. 5. Blowoff limits of non-premixed ammonia/hydrogen flames at the inlet temperature of **300 K (S = 0.87)**.

plotted in Fig. 5. The region between the rich and lean blowoff limits is the region of stable non-premixed ammonia/hydrogen flame. It can be seen that hydrogen involvement expands the stable range of ammonia flames, and it has more pronounced effect on the lean blowoff limits than that on rich blowoff limits. For example, the stable range (global equivalence ratio) for 80% NH_3/ 20% H_2 flame is $0.576 - 1.084$ while that for 70% NH_3/ 30% H_2 is $0.388 - 1.141$. Due to the limitation of the maximum air flow rate, 60% NH_3/ 40% H_2 flame burns steadily at 6.870 g/s and its lean blowoff limit can be extended further. Increasing hydrogen addition is effective in igniting the fuel mixture, generating sufficient heat and maintain a stable flame, especially under lean-burn conditions due to better mixing with air; however, the effect is weakened under rich-burn conditions as less oxidant exits and combines with the fuel. The finding is comparable with the conclusions drawn from the lean blowoff limits of premixed ammonia/hydrogen flames [11]. The trend of lean blowoff limit in non-premixed ammonia/hydrogen flames is consistent with that of the premixed ammonia/hydrogen flames, i.e., the lean blowoff limit is gradually decreased as hydrogen blending ratio increases.

The effect of inlet temperature on the blowoff limits of non-premixed 60% NH_3/ 40% H_2 flame is presented in Fig. 6. It is noticed that the lean blowoff limits of non-premixed 60% NH_3/ 40% H_2 can be further extended because the flames under room temperature and elevated temperature are still robust with the maximum air mass flow rate available in the laboratory. Therefore, only the effect of inlet temperature on the rich blowoff limit can be observed. The ranges to achieve the stable flames are widened when rising the inlet temperature. For instance, the rich blowoff limit is extended from 1.204 to 1.290 when the inlet temperature rises from 300 K to 400 K and it extends further to 1.505 when the inlet air temperature rises to 435 K and the inlet fuel temperature rises to 475 K. A dimensionless number, Damköhler number (Da), has to be greater than unity to obtain a stable flame [42]. Damköhler number is determined by the ratio of the characteristic mixing time to the characteristic chemical reaction time. An increase in the inlet temperature enhances the chemical reaction rate and burning rate, which reduces the chemical reaction time. As a result, Damköhler number is greater with a high inlet gas temperature and the stable range of the flame was extended.

Adding swirlers is generally considered as an effective way to increase the mixing ratio of fuel and oxidizer in the shear layer region. Therefore, in this work, three swirlers, *S(a), S(b), S(c)*, are employed to

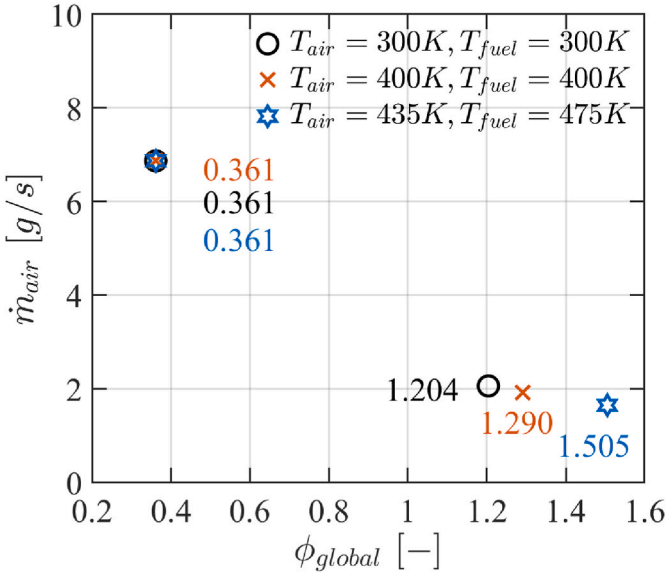

Fig. 6. Blowoff limits of non-premixed flames **60% NH_3/ 40% H_2** under different inlet gas temperature (**$S = 0.87$**).

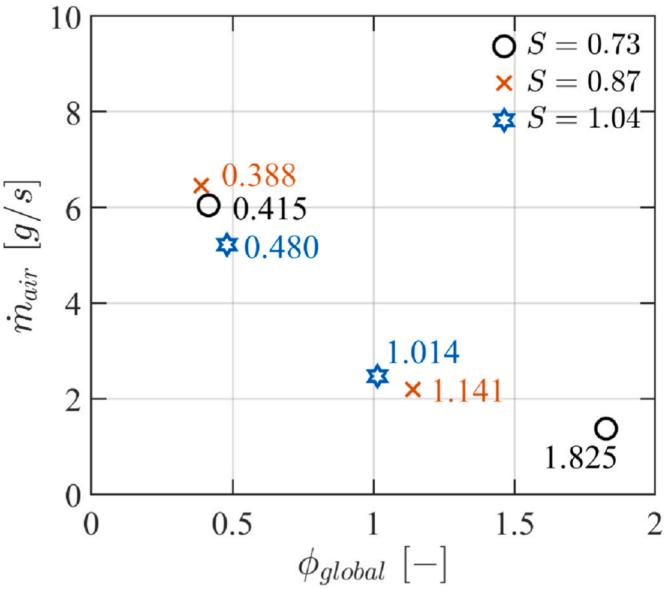

Fig. 7. Blowoff limits of non-premixed **70% NH_3/ 30% H_2 flames with different swirl numbers at the inlet temperature of 300 K.**

investigate the effect of swirl numbers on the blowoff limits of non-premixed ammonia/hydrogen flames. Fig. 7 demonstrates the increase in the swirl number shortens the flame stability range considerably for non-premixed 70% NH_3/ 30% H_2 flames. The effect on the rich blowoff limits is more pronounced than the effect on the lean blowoff limits. The effect of swirl numbers on the blowoff limits of premixed ammonia/methane was also analysed by Zhang et al. [43]. It was reported that when the swirl number was changed between $0.42, 0.71, 1.27$, the lean and rich blowoff limits almost stayed unchanged in premixed ammonia flames; however, an apparent extension on the lean blowoff limits was observed in premixed 50% NH_3/ 50% CH_4 flames.

3.2. Emissions

3.2.1. Emission performance of different hydrogen blending ratios at different global equivalence ratios

Although no carbon emissions will be emitted from non-premixed ammonia/hydrogen combustion, nitric oxides, ammonia slip and unburnt hydrogen can be produced, all of which are harmful to the atmosphere. A clear knowledge of emission characteristics of non-premixed ammonia/hydrogen combustion is beneficial for emission control when designing the industrial applications powered by ammonia and hydrogen. Therefore, emissions of NO, NO_2, NH_3, H_2 are emphasised in this section and all the results have been normalised to the standard oxygen level, 15%(vol).

Fig. 8 depicts the effects of global equivalence ratios and hydrogen blending ratios on the emissions of non-premixed ammonia/hydrogen flames. When the hydrogen blending ratio is 20% and 30%, it can be seen that NO, NO_2 emissions increase when the global equivalence ratio rises from $0.6 - 0.8$, reach the peak at the global equivalence ratio of 0.8 with about 100 $ppmvd@15\%O_2$ for NO emission and about 35 $ppmvd@15\%O_2$ for NO_2 emission and decrease with further increase in the global equivalence ratio. A similar trend is also observed when the hydrogen blending ratio is 40%, but both NO and NO_2 emissions are much higher at a low global equivalence ratio compared to the results with hydrogen blending ratio at 20% and 30%. The maximum NO and NO_2 emissions reach approximately 350 $ppmvd@15\%O_2$ and 60 $ppmvd@15\%O_2$, respectively. There are dramatic reductions for NO and NO_2 emission when the global equivalence ratio is close to the unity. NO and NO_2 emission were almost the same low value under fuel-rich conditions when hydrogen blending ratio was at 20%, 30% and 40%.

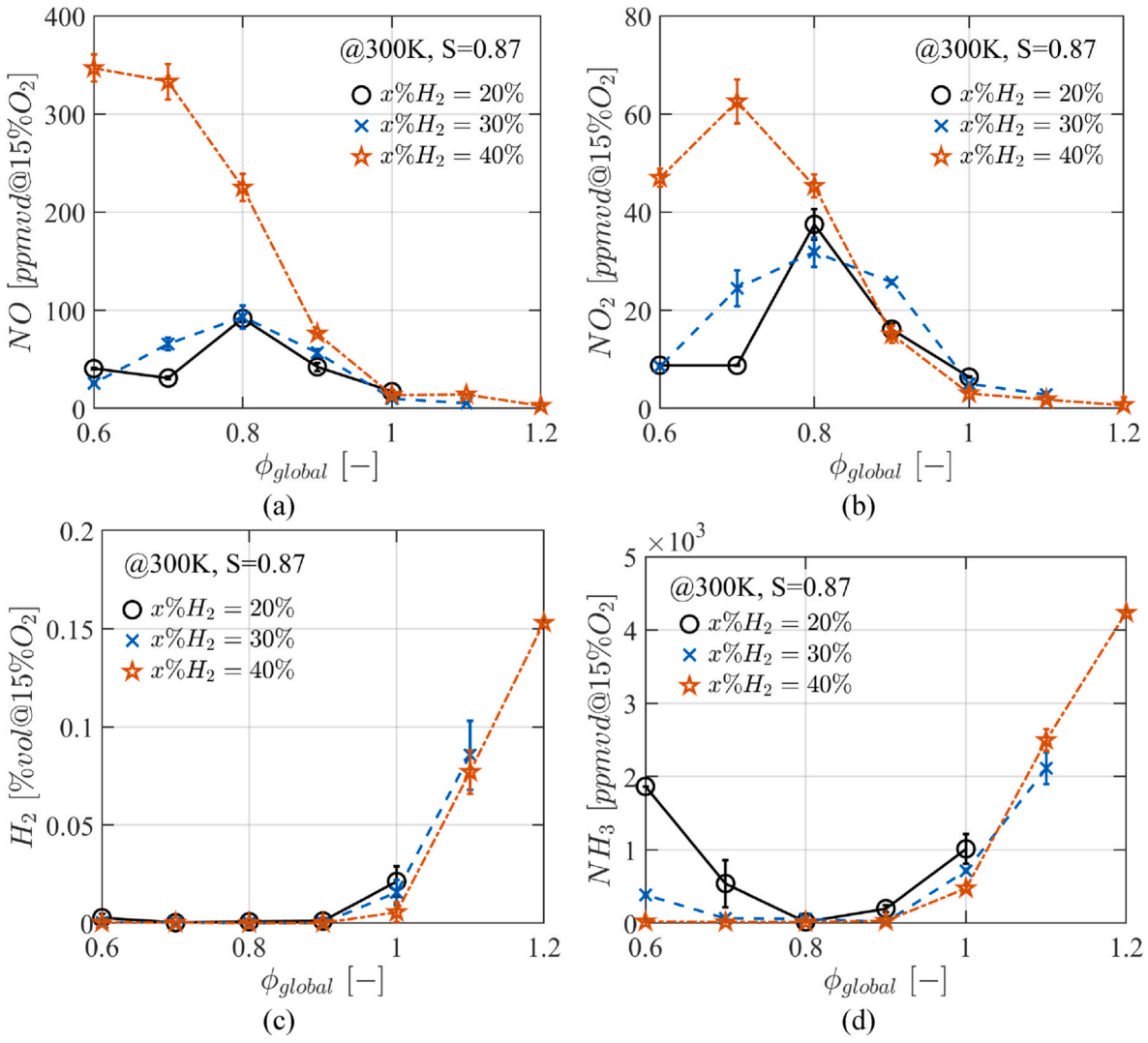

Fig. 8. Emissions of non-premixed ammonia/hydrogen flames versus various global equivalence ratios at different hydrogen blending ratios.

In ammonia combustion, NO and NO_2 formations and consumptions are mainly associated with the flame temperature (thermal NO_x route) and concentrations of $O/H/OH$ radicals in the flame (fuel-bound NO_x route). When the global equivalence ratio is far-lean, the flame temperature is very low which suppressed NO and NO_2 production. As the global equivalence ratio increases but below the unity, fuel-bound NO_x ($HNO + H = NO + H_2, HNO + OH = NO + H_2O$) is the main pathway for NO_x formation. Meanwhile, the flame temperature is relatively higher which induced further NO_x emission caused by the thermal NO_x formation. This can be explained the reason of low emissions of NO, NO_2 found at a very low equivalence ratio and the increase of emissions with the global equivalence ratio increasing to one. Conversely, under fuel-rich conditions, the fuel-bound route for NO_x formation is inhibited as the concentrations of $O/H/OH$ radicals are decreased. Instead, the thermal NO_x route for NO_x consumption is promoted and dominate to consume NO_x, resulting the reduction in NO and NO_2 emissions when the global equivalence ratio is greater than one.

Although NO and NO_2 emissions keep decreasing under fuel-rich conditions, the unburnt fuel including hydrogen and ammonia rises significantly. At the global equivalence ratio of 1.2, ammonia slip is over 4000 $ppmvd$@15%O_2 while unburnt hydrogen is over 0.15%vol@15%O_2 at the exhaust. Combustion efficiency is an indicator of the combustion completeness. The unburnt fuels and products in the exhaust gas are considered. Taking the combustion efficiency into account, the optimal emission control occurred at stoichiometric condition. Relative low emissions including NO_x and unburnt fuel were also found at far-lean global equivalence ratio with hydrogen blending ratio at 20% and 30%, but the flame robustness of ammonia and hydrogen at far-lean global equivalence ratio should be considered and investigate further.

Surprisingly, changes in hydrogen blending ratios have no significant impact on the unburnt hydrogen over the wide range of the global equivalence ratios. However, due to the flame temperature elevated by more hydrogen involvement, thermal NO_x formation is greatly affected. The elevated flame temperature also improves the ammonia fuel consumption. Consequently, increased NO and NO_2 as well as reduced ammonia slip at the exhaust were observed as more hydrogen was blended with ammonia. However, the effect is weakened considerably when the global equivalence ratio is above the unity. It indicates that more hydrogen blending ratios provide less penalty on emissions under fuel-rich conditions.

3.2.2. *Emission performance at different inlet temperatures*

In Fig. 9, variations of emissions for non-premixed 60% NH_3/ 40% H_2 flames are presented with the constant global equivalence ratio at 1.1 and swirl number at 0.87. The inlet fuel temperature varied from 300 to 400 K and the inlet air temperature varied from 300 to 350 K. It was well known that increasing the inlet temperature improves the flame temperature and chemical reaction rate. According to the Zel'dovich

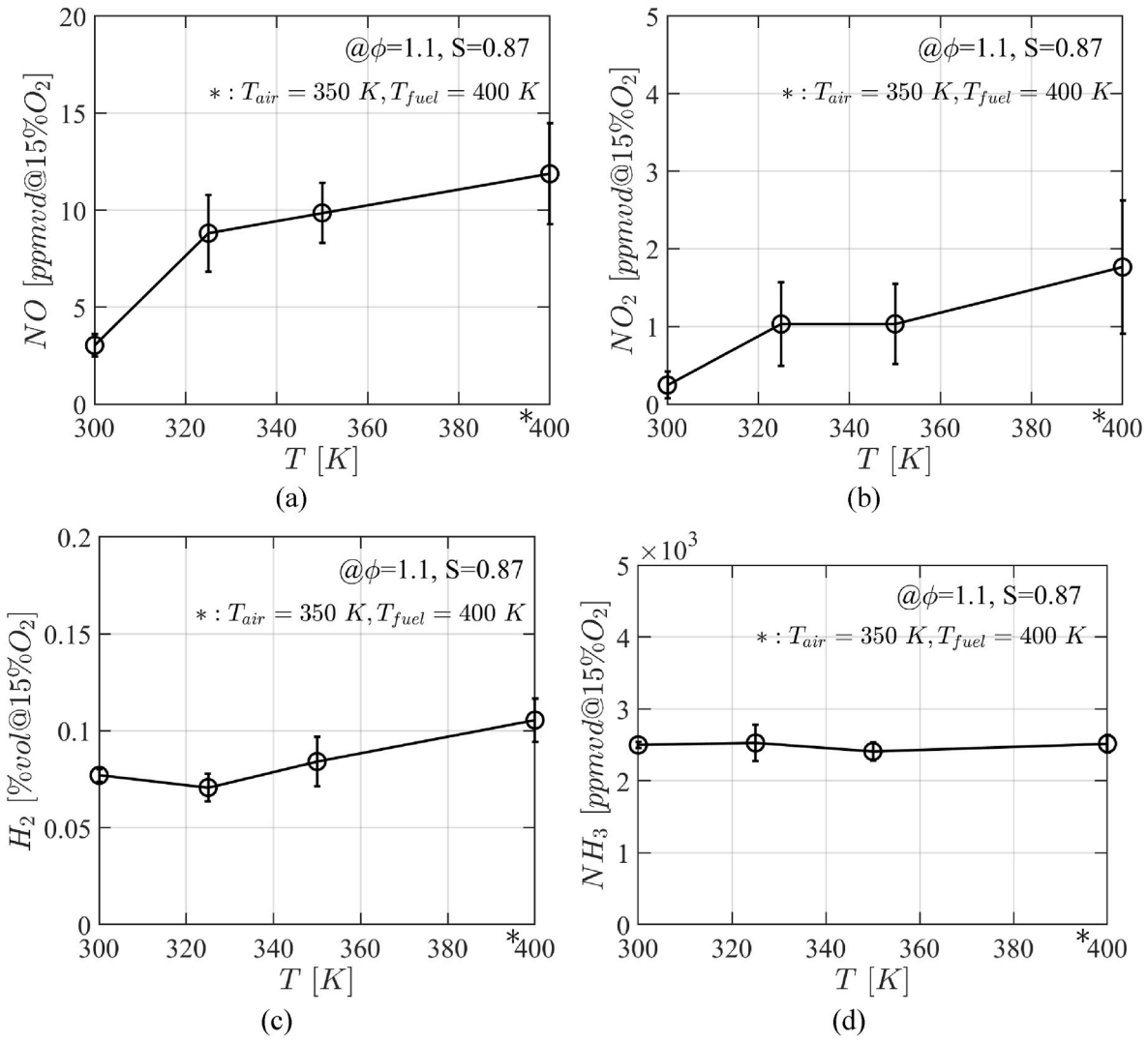

Fig. 9. Emissions of non-premixed **60%** NH_3/ **40%** H_2 flames versus different inlet temperature.

mechanism, when the temperature is above 1800 *K*, NO_x formation through thermal NO_x route is promoted. Valera-Medina et al. [17] investigated premixed ammonia/hydrogen flames using 0D Gaseq analysis, finding NO_x concentration of flue gas was increased as the inlet temperature increase from 300 to 900 *K* at 10 *bar*. However, the experimental results in the present work show the lifted inlet temperature had no obvious impact on the emission at the global equivalence ratio of 1.1. The measured inner wall temperature was increased by approximately 46 *K* for every 25 *K* increase in the inlet temperature. The moderate effect of increasing the inlet gas temperature on the inner wall temperature could be owing to the heat loss from the sizeable optical window and the insufficient increase in the inlet temperature. This suggests that the increase in the flame temperature not be significant in showing the profound difference in emissions. The conjecture of flame temperature was verified in section 3.3 OH^* chemiluminescence, Fig. 14.

3.2.3. Emission comparison under the wall insulated and non-insulated conditions

As temperature plays a key role in the flame and affects emissions considerably, the effect of wall condition on emissions of non-premixed ammonia/hydrogen combustion has been investigated. The combustion chamber was insulated with silicate ceramic fibre blankets to compare the emission results between insulated wall conditions and non-insulated wall conditions. Fig. 10 illustrates the emissions for non-premixed 70% NH_3/ 30% H_2 flames with the inlet gas temperature of 300 *K* under insulated wall condition and non-insulated wall condition. The results show that a substantial growth of up to 107% (φ_{global} = 0.8) in *NO* emission and up to 92% (φ_{global} = 0.8) in NO_2 emission, alongside a notable reduction of up to 44% (φ_{global} = 1.1) in unburnt ammonia at the exhaust, when the combustion chamber is converted from non-insulated to insulated. Meanwhile, unburnt hydrogen kept almost the same. It suggests a great heat loss from the optical window and combustion chamber. The great heat loss, especially in the region close to the wall, considerably suppresses the generation of O/H radicals which are mainly yielded by the chain branching reaction, $H + O_2 \rightarrow OH + O$ [44]. Thus, thermal NO_x generation is suppressed. The substantial ammonia concentration at the exhaust suggests further low NO_x generation from ammonia through fuel-bound NO_x route. The emission trends are consistent with the study on non-premixed ammonia/air flames that have been examined experimentally with non-insulated quartz glass liner, non-insulated steel liner and insulated steel liner [45].

3.2.4. Emission performance at different swirl numbers

Three swirlers with different vane angles were tested. Fig. 11 demonstrates the emissions of non-premixed 70% NH_3/ 30% H_2 flames with various swirl numbers. Due to the flame stability difference using different swirl numbers, flames measured with small swirl number

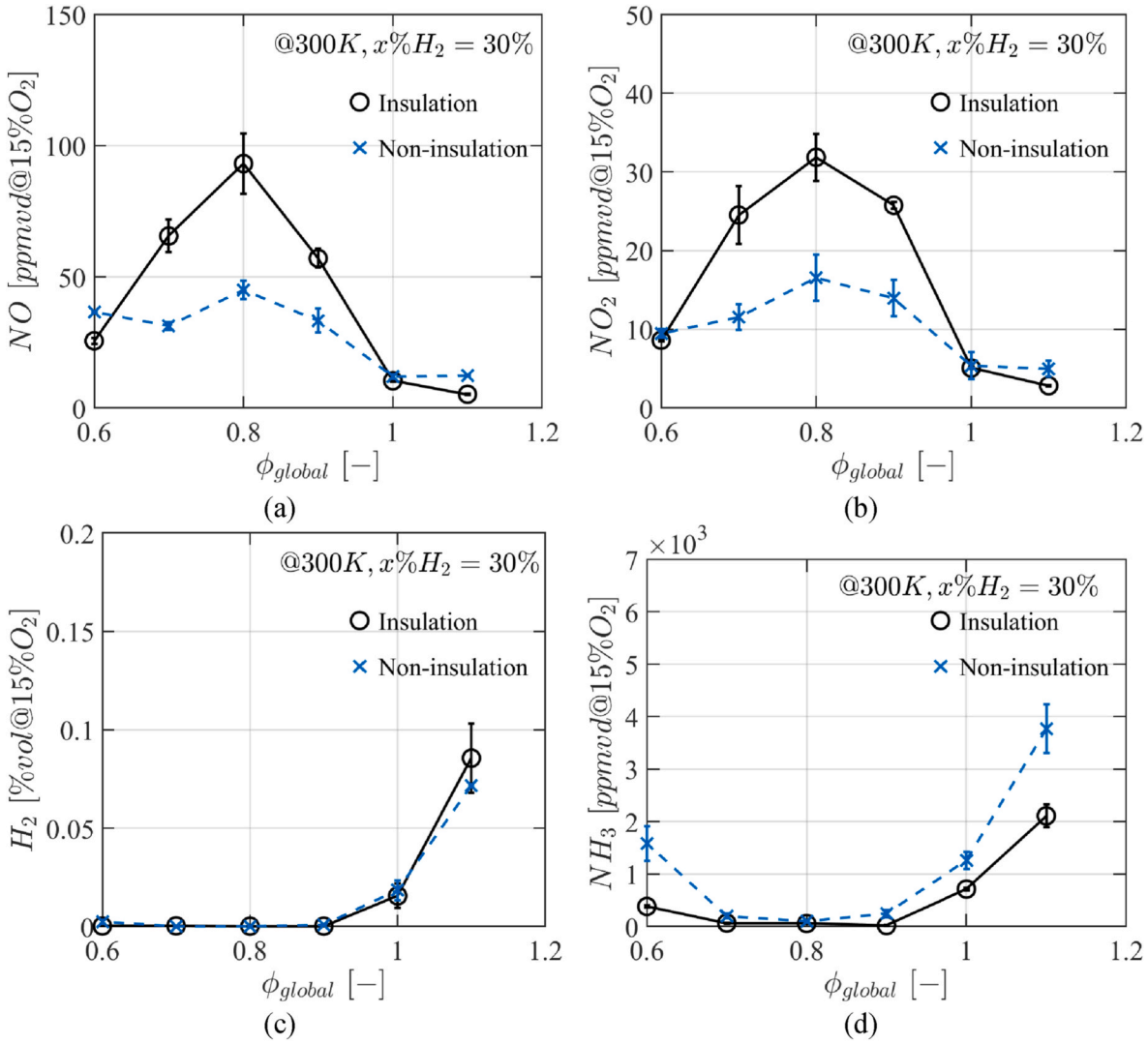

Fig. 10. Emissions of non-premixed **70%** NH_3 / **30%** H_2 flames versus various global equivalence ratios under insulated and non-insulated wall conditions ($S = 0.87$).

provide a wider range of emission results. It is found that the change in the swirl number has a moderate effect on the NO_x emission, although a slight reduction of *NO* and NO_2 concentration with swirler number at 0.87 and 1.04 was observed when the global equivalence ratio was greater than 0.8. Under far-lean conditions, unburnt hydrogen concentration at the exhaust is almost unaffected by swirl numbers while unburnt ammonia concentration at the exhaust is reduced considerably. For instance, at the global equivalence ratio of 0.6, the unburnt ammonia was 1880 *ppmvd*@15%O_2 with swirl number at 0.73, 1580 *ppmvd*@15%O_2 with swirl number at 0.87 and 887 *ppmvd*@15%O_2 with swirl number at 1.04. In the premixed 30% NH_3/ 70% CH_4 flames, it was reported in the literature by conducting a large eddy simulation that a decreased *NO* emission was achieved by increasing the swirl number from 0.58 to 0.99, and when the swirl number was greater than 0.76, less effect was observed on *NO* reduction [46]. It suggests there is potentially an optimal swirl number for *NO* emission control in non-premixed ammonia/hydrogen flames. Under the fuel-rich conditions, both the concentrations of unburnt hydrogen and ammonia were increased dramatically with a higher swirl number. As the angle of fuel nozzle is 45°, the vane angle of swirler at 40° ($S = 0.73$) enables the fuel and air to be mixed near the nozzle. The vane angle of swirler at 50° ($S = 1.04$) provides a stronger swirling flow but the mixing flow is being pushed closer to the cold wall. The mixing flow is burnt near the nozzle but the mixing flow close to the cold wall is likely to be pushed to the exhaust without reacting. The behaviour became stronger with more fuel dominate in the chamber, which led to less unburnt fuel (hydrogen and ammonia) with a low swirl number under fuel-rich condition. The effect of swirl numbers on unburnt fuel emission became greater when the global equivalence ratio was further increased.

3.3. OH^* chemiluminescence

Chemiluminescence of a flame is the spontaneous emission of light that occurs when a chemical species descends from the excited to the ground state. Excited hydroxyl (OH^*) chemiluminescence is recognised as an important parameter to understand physical properties without interfere with the actual flame, e.g. flame structure, relationship with *NO* concentration. In this section, a thousand of images of OH^* chemiluminescence were taken for each case to gain the knowledge qualitatively and quantitively. For the distribution of OH^* chemiluminescence, normalisation was conducted to the image data by dividing by the maximum intensity of each case and rescaling to the same range shown in the colour bar. Therefore, it is noted that the value (II_{OH^*}) does not represent the absolute value.

Fig. 12(a) shows the OH^* chemiluminescence profiles of the non-premixed 60% NH_3/ 40% H_2 flame with various global equivalence ratio in the range of $0.6 - 1.2$ measured at the room temperature with the swirl number of 0.87. Owing to the axis symmetry of the image, only

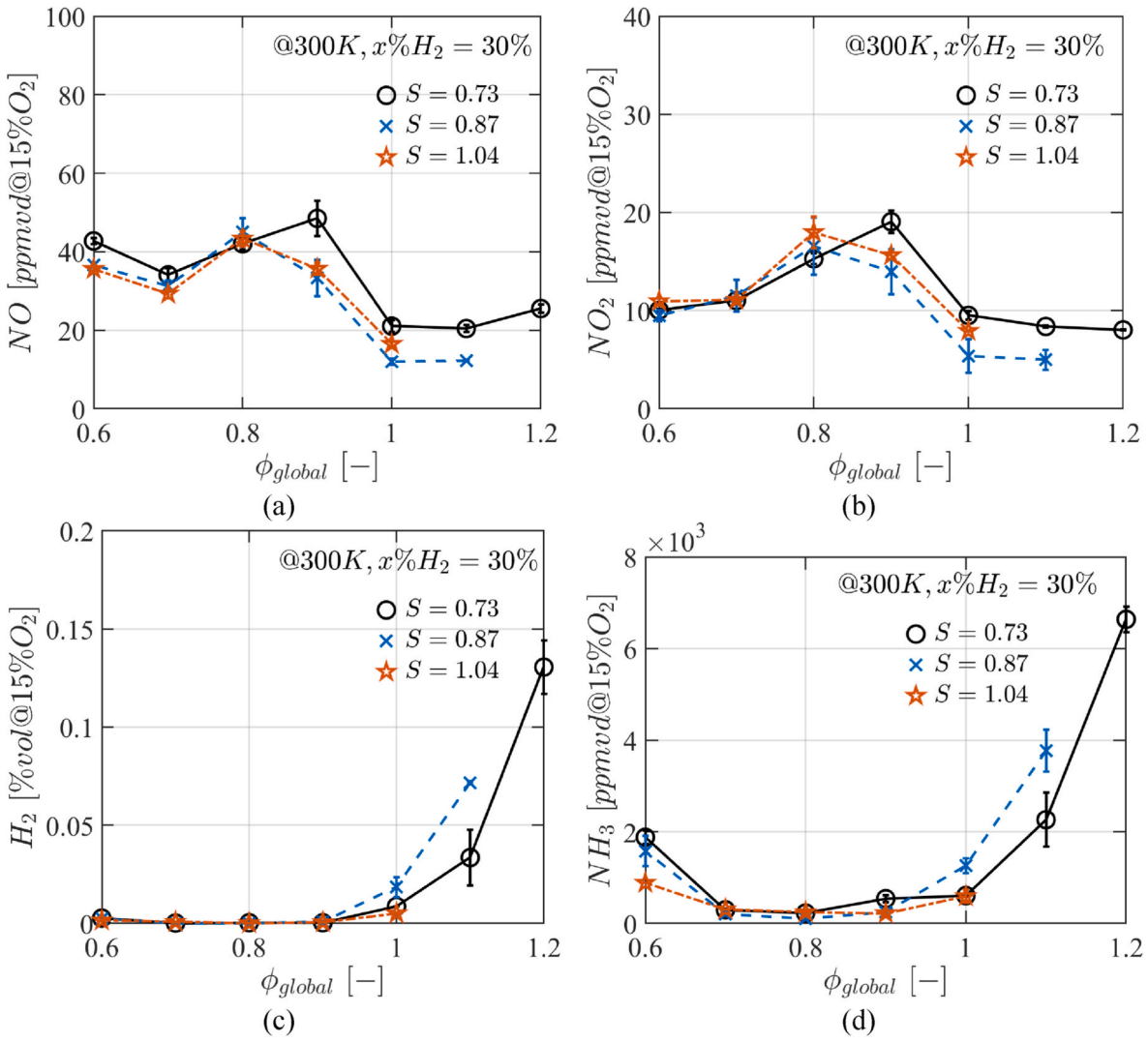

Fig. 11. Emissions of non-premixed **70%** NH_3/ **30%** H_2 flames versus various global equivalence ratios with different swirl numbers.

the top half of each image is rotated for analysis. From the perspective of topology in each case, it is found that the OH^* concentration was generally located at the upstream close to the nozzle in all cases and it was moved further away from the nozzle when the global equivalence ratio increased. Furthermore, OH^* chemiluminescence distribution was expanded as the flame became richer. The phenomenon was consistent with the observation of flame shape. At the far-lean conditions, the flame height of ammonia/hydrogen was short and orangish. As less oxidizer was participated in the reaction, the flame height became longer and turned to yellow-ish. It demonstrates that the feature of OH^* chemiluminescence distribution that can be used to identify flame shape can also be extended to non-premixed ammonia and hydrogen flames. Fig. 12 (b) reveals the OH^* intensity results with the respect to the global equivalence ratios. It can be seen that the OH^* intensity trend is compatible with the trend in *NO* emission in Fig. 8 (a). Hydroxyl radical plays a critical role in fuel-bound *NO* formation ($HNO + OH = NO + H_2O$) and fuel-bound *NO* formation dominates in the *NO* emission under fuel-lean conditions. Under fuel-rich conditions, fuel-bound *NO* formation route is inhibited due to the insufficient $O/H/OH$ radicals. Therefore, hydroxyl radical and excited hydroxyl radical measurement reflects nitric oxide concentrations at the post-flame zone. The findings agree with the results observed with premixed ammonia/air flames and partially premixed ammonia/hydrogen flames in the literature [22].

It is depicted in Fig. 13(a) that OH^* chemiluminescence images of the non-premixed ammonia/hydrogen flames with hydrogen blending ratio at 20%, 30% and 40% at stoichiometric condition. The result shows that OH^* chemiluminescence near the nozzle region was evidently enlarged as more hydrogen was involved in the fuel blends. For the case of non-premixed 80% NH_3/ 20% H_2 flame, OH^* is intense at the region near the nozzle and downstream, showing a weak flame behaviour. It agrees with the results in Fig. 5 that the rich blowoff limit for this case is slightly above the global equivalent ratio at 1.0. With the increase of the hydrogen blending ratio, the OH^* radicals became more concentrated near the nozzle and the flame became more robust. As illustrated in Fig. 13 (b), the OH^* intensity is about 37% higher at a hydrogen blending ratio of 20% than at a hydrogen blending ratio of 30% that is almost the same as at the hydrogen blending ratio of 40%. In comparison with results in Fig. 8, the change in OH^* intensity is consistent with the change in *NO* emission at the global equivalence ratio of 1.0. Hydrogen involvement lifted the flame temperature, an increase in *NO* emission via thermal *NO* production is expected. However, much higher OH^* concentration was found in 80% NH_3/ 20% H_2, indicating that the fuel-bound *NO* route still substantially contributes to *NO* production and it is slightly greater than the effect of increasing the hydrogen blending ratio up to 40% when the global equivalence ratio was at 1.0.

In Fig. 14(a), the distributions of OH^* chemiluminescence of non-premixed 60% NH_3/ 40% H_2 flames are presented with different inlet temperature at the global equivalence ratio of 1.1. The flame shape

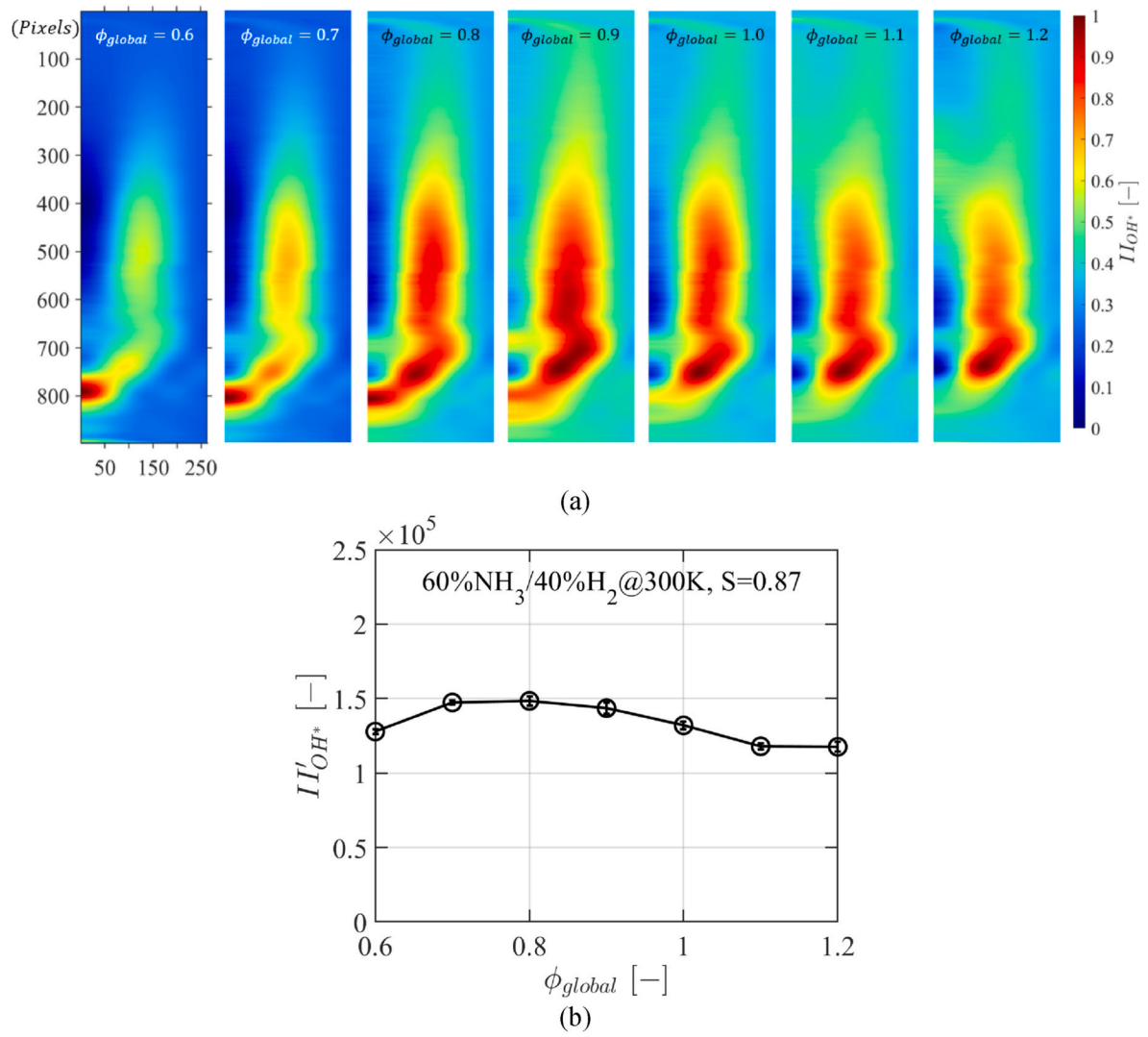

Fig. 12. (a) OH^* chemiluminescence profiles (normalised colormap applied) and (b) OH^* intensity for non-premixed **60% NH_3/ 40% H_2** flames with various global equivalence ratios ($\boldsymbol{T = 300\,K, S = 0.87}$).

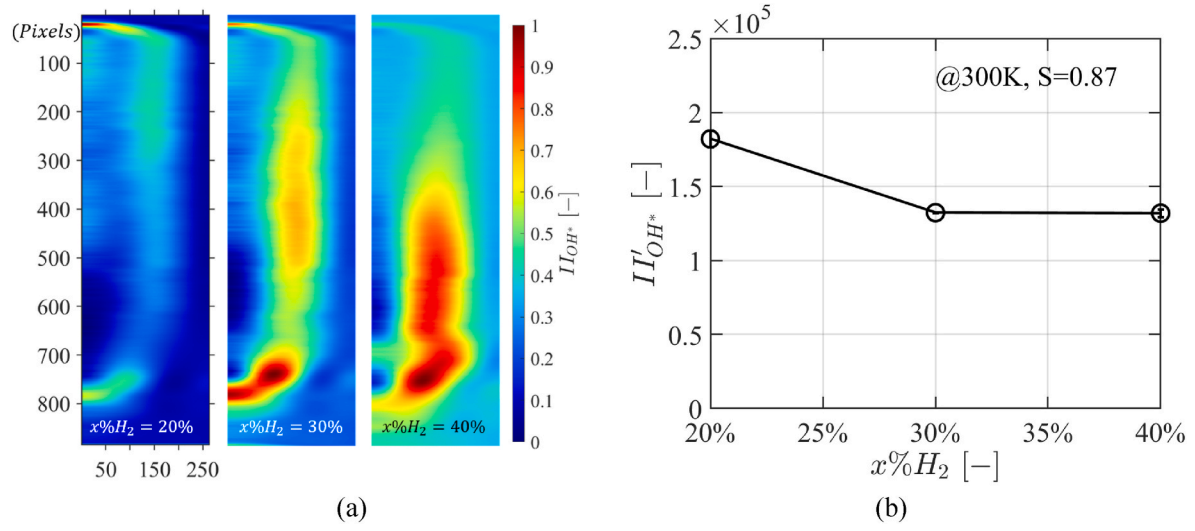

Fig. 13. (a) OH^* chemiluminescence profiles (normalised colormap applied) and (b) OH^* intensity for non-premixed flames with various hydrogen blending ratios ($\boldsymbol{\varphi_{global} = 1, T = 300\,K, S = 0.87}$).

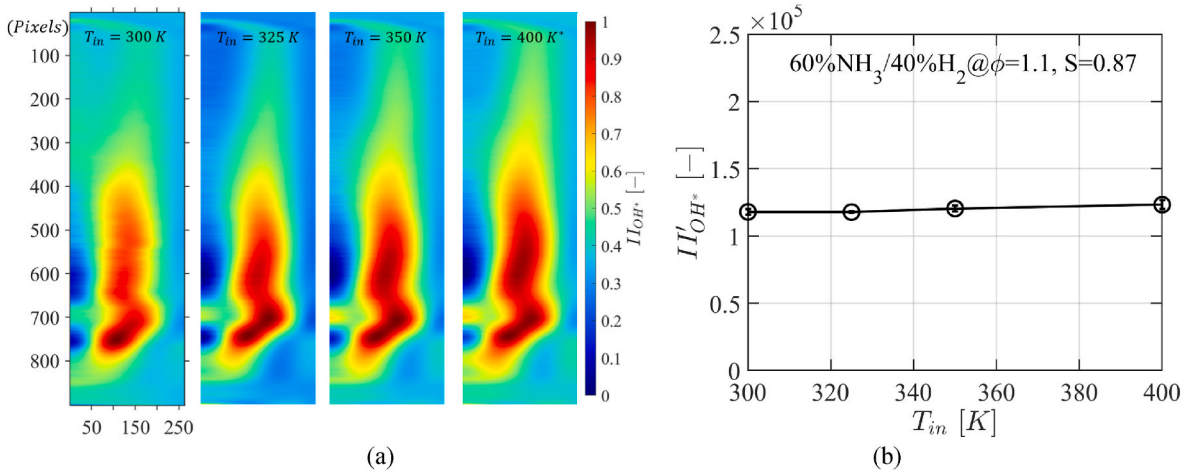

Fig. 14. (a) OH^* chemiluminescence profiles (normalised colormap applied) and (b) OH^* intensity for non-premixed **60%** NH_3/ **40%** H_2 flames with various inlet temperature ($\varphi_{global} = 1.1, S = 0.87$).

remained almost unchanged, but the regions of the peak OH^* concentration (deep red) was expanded. Fig. 14(b) also reflects rising the inlet temperature has no significant effect on the OH^* intensity, with a slight increase observed. It indicates that there was no considerable change in the flame temperature in the current experiment as the inlet air temperature rising from room temperature to 350 K and inlet fuel temperature rising to 400 K. Therefore, it can explain the result of NO emission in Fig. 9 (a) which was found almost the constant.

Three different swirlers were changed to create various flow recirculation in the combustor. The profiles of OH^* chemiluminescence of non-premixed 70% NH_3/ 30% H_2 flames with different swirlers are demonstrated in Fig. 15(a) at the stoichiometric condition under the room temperature. As the vane angle of the swirler varied from 40° to 50 °, the angle of the OH^* concentration upstream was deflected, which helped the circulation and mixing ratio of the fuel and air near the nozzle. Additionally, with a higher swirl number, OH^* concentration in the region near the nozzle and transition region expanded and showing a more strengthened flame. For instance, when the swirl number reached 1.04, the red marked OH^* chemiluminescence was from the nozzle all the way downstream. In Fig. 15 (b), it is notable that the OH^* intensity decreased and then increased significantly as the swirl number rose from 0.73 to 1.04. However, the emission results in Fig. 11 (a) show a higher NO emission was found at the swirl number of 0.73, which does not match the results of OH^* intensity under the same condition. It is necessary to conduct a further spatial and temporal information investigation into the pathways of NO formation to understand the reasons behind it.

4. Conclusions

Combustion and emission characteristics of non-premixed ammonia/hydrogen flames were studied experimentally with a swirl-enhanced combustor test rig. The blowoff limits were identified firstly. The effects of global equivalence ratios $(0.6 - 1.2)$, hydrogen blending ratios $(20\% - 40\%)$, inlet gas temperatures $(300 - 400\,K)$, swirl numbers $(0.73, 0.87, 1.04)$ and combustion chamber wall insulation conditions on emissions (NO, NO_2, NH_3, H_2) were analysed. Excited hydroxyl radical (OH^*) chemiluminescence imaging technology was unveiled. The main findings are summarised below.

(1) Taking the combustion efficiency into account, the optimal emission control occurred at stoichiometric condition. At far-lean global equivalence ratios, NO_x and unburned fuel also showed

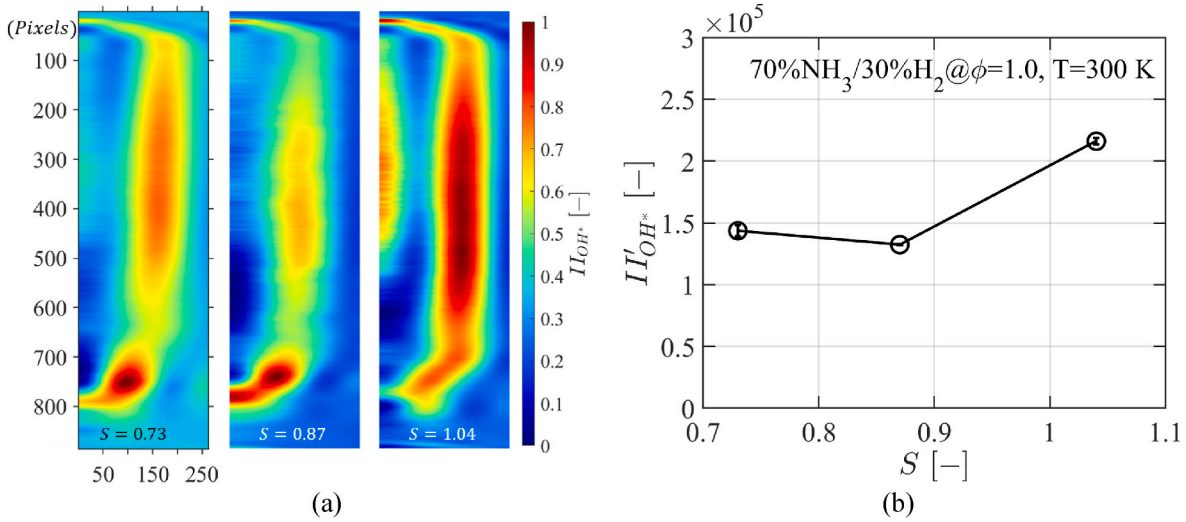

Fig. 15. (a) OH^* **chemiluminescence profiles (normalised colormap applied) and (b)** OH^* **intensity for non-premixed 70%** NH_3/ **30%** H_2 **flames with various swirl numbers** ($\varphi_{global} = 1.0, T = 300\,K$).

relatively low emissions with hydrogen blending ratio at 20% and 30%; however, flame stability is of concern.

(2) Robust flames were obtained at hydrogen blending ratio over 20%. More hydrogen involvement resulted in the increase of *NO* and NO_2 emissions and the decreased ammonia slip. However, the effect was weakened under fuel-rich conditions.

(3) With the global equivalence ratio of 1.1, the rising inlet gas temperature has a marginal effect on emissions due to the heat loss from the combustor wall and optical windows. After the non-insulation rig was converted to the wall insulated combustor, *NO* and NO_2 emissions increased by a maximum of 107% and 92%, respectively, despite a reduction in ammonia slip of up to 44%.

(4) In the current combustor setup, when the global equivalence ratio above 0.8, *NO* and NO_2 emissions were lower with the swirl number of 0.87 and 1.04 than that with the swirl number of 0.73. This suggested there is an optimal swirl number for NO_x control and its value changes depending on the geometry and size of combustor.

(5) OH^* chemiluminescence distribution can effectively identify the shape of non-premixed ammonia and hydrogen flames. The trend of OH^* intensity was consistent with the results of *NO* emissions at the same swirl number.

Declaration of competing interest

The authors declare that they have no known competing financial interests or personal relationships that could have appeared to influence the work reported in this paper.

Acknowledgements

The authors are grateful for the financial support from EPSRC (Engineering and Physical Sciences Research Council, United Kingdom) through the project 'Powering Carbon-free Autonomous Shipping: Ammonia/Hydrogen dual-fuelled Linear Engine-Generator' (EP/S00193X/2) and the project 'Premixed Combustion Flame Instability Characteristics' (EP/W002299/1). The authors also thank for the project support from Merchant Marine College of Shanghai Maritime University.

Nomenclature

NTP	Normal Temperature and Pressure
GTRC	Gas Turbine Research Centre
CRN	Chemical Reactor Network
MFCs	Mass Flow Controllers
LHVs	Lower Heating Values
PDD	Pulse Discharge helium ionisation Detector
TCD	Thermal Conductivity Detector
S	Swirl number (–)
Da	Damköhler number (–)
D_i	Inner diameter of swirler (mm)
D_o	Outer diameter of swirler (mm)
α	Vane angle of swirler (°)
P	Total input thermal power (kW)
$\dot{m}_{fuel}$	Mass flow rate of fuel blends (g/s)
$\dot{m}_{air}$	Mass flow rate of air (g/s)
$x[NH_3]$	Mole fraction of ammonia in the fuel blends (–)
$x[H_2]$	Mole fraction of hydrogen in the fuel blends (–)
φ_{global}	Global fuel-air equivalence ratio (–)
$x\%H_2$	Hydrogen blending ratio (–)
ppm_{norm}	Normalised emission concentration ($ppmvd@15\%O_2$)
ppm_{mea}	Measured emission concentration ($ppmvd$)
O_{2mea}	Measured oxygen concentration in the exhaust gases ($ppmvd$)
$\mathrm{II}_{\mathrm{OH}^*}$	Normalised OH^* intensity (–)
$\mathrm{II}'_{\mathrm{OH}^*}$	OH^* intensity before normalisation (–)
$\bar{\mathrm{I}}_{OH^*_{ij}}$	OH^* intensity of the i^{th} column and the j^{th} row (–)
T_{fuel}	Inlet fuel temperature (K)
T_{air}	Inlet air temperature (K)

References

[1] Morgan E, Manwell J, McGowan J. Wind-powered ammonia fuel production for remote islands: a case study. Renew Energy 2014;72:51–61.
[2] Bicer Y, Dincer I, Zamfirescu C, Vezina G, Raso F. Comparative life cycle assessment of various ammonia production methods. J Clean Prod 2016;135:1379–95.
[3] MacFarlane DR, Cherepanov PV, Choi J, Suryanto BHR, Hodgetts RY, Bakker JM, et al. A roadmap to the ammonia economy. Joule 2020;4:1186–205.
[4] Banares-Alcantara R, Dericks G, Fiaschetti M, Grunewald P, Lopez JM, Tsang E, et al. Analysis of islanded NH3-based energy storage system 2015.
[5] Valera-Medina A, Xiao H, Owen-Jones M, David WIF, Bowen PJ. Ammonia for power. Prog Energy Combust Sci 2018;69:63–102.
[6] NcfB Information. PubChem compound summary for CID 222. Ammonia 2022:2022.
[7] Lee JH, Lee SI, Kwon OC. Effects of ammonia substitution on hydrogen/air flame propagation and emissions. Int J Hydrogen Energy 2010;35:11332–41.
[8] Ichikawa A, Hayakawa A, Kitagawa Y, Amila Somarathne Kd Kunkuma, Kudo T, Kobayashi H. Laminar burning velocity and Markstein length of ammonia/hydrogen/air premixed flames at elevated pressures. Int J Hydrogen Energy 2015;40:9570–8.
[9] Hayakawa A, Goto T, Mimoto R, Arakawa Y, Kudo T, Kobayashi H. Laminar burning velocity and Markstein length of ammonia/air premixed flames at various pressures. Fuel 2015;159:98–106.
[10] Joo JM, Lee S, Kwon OC. Effects of ammonia substitution on combustion stability limits and NOx emissions of premixed hydrogen–air flames. Int J Hydrogen Energy 2012;37:6933–41.

[11] Tang G, Jin P, Bao Y, Chai WS, Zhou L. Experimental investigation of premixed combustion limits of hydrogen and methane additives in ammonia. Int J Hydrogen Energy 2021;46:20765–76.
[12] Khateeb AA, Guiberti TF, Wang G, Boyette WR, Younes M, Jamal A, et al. Stability limits and NO emissions of premixed swirl ammonia-air flames enriched with hydrogen or methane at elevated pressures. Int J Hydrogen Energy 2021;46:11969–81.
[13] Lhuillier C, Brequigny P, Lamoureux N, Contino F, Mounaïm-Rousselle C. Experimental investigation on laminar burning velocities of ammonia/hydrogen/air mixtures at elevated temperatures. Fuel 2020;263.
[14] da Rocha RC, Costa M, Bai X-S. Chemical kinetic modelling of ammonia/hydrogen/air ignition, premixed flame propagation and NO emission. Fuel 2019;246:24–33.
[15] Wei X, Zhang M, Wang J, Huang Z. Investigation on lean blow-off characteristics and stabilization mechanism of premixed hydrogen enhanced ammonia/air swirl flames in a gas turbine combustor. Combust Flame 2023:249.
[16] Zhen HS, Tan K, Liu XY, Wei ZL, Wang XC, Liu WF. Experimental investigation on ammonia-hydrogen-air Bunsen flames for impingement heating applications. Int J Hydrogen Energy 2024;49:547–59.
[17] Valera-Medina A, Pugh DG, Marsh P, Bulat G, Bowen P. Preliminary study on lean premixed combustion of ammonia-hydrogen for swirling gas turbine combustors. Int J Hydrogen Energy 2017;42:24495–503.
[18] Valera-Medina A, Gutesa M, Xiao H, Pugh D, Giles A, Goktepe B, et al. Premixed ammonia/hydrogen swirl combustion under rich fuel conditions for gas turbines operation. Int J Hydrogen Energy 2019;44:8615–26.
[19] Chen D, Li J, Li X, Deng L, He Z, Huang H, et al. Study on combustion characteristics of hydrogen addition on ammonia flame at a porous burner. Energy 2023;263.
[20] Tong J, Cai T, Zhao D. Optimizing thermal performances and NOx emission in a premixed ammonia-hydrogen blended meso-scale combustor for thermophotovoltaic applications. Int J Hydrogen Energy 2023;48:30191–204.
[21] Zhu X, Khateeb AA, Guiberti TF, Roberts WL. NO and OH* emission characteristics of very-lean to stoichiometric ammonia–hydrogen–air swirl flames. Proc Combust Inst 2021;38:5155–62.
[22] Pugh D, Runyon J, Bowen P, Giles A, Valera-Medina A, Marsh R, et al. An investigation of ammonia primary flame combustor concepts for emissions reduction with OH*, NH2* and NH* chemiluminescence at elevated conditions. Proc Combust Inst 2021;38:6451–9.
[23] Okafor EC, Somarathne KDKA, Hayakawa A, Kudo T, Kurata O, Iki N, et al. Towards the development of an efficient low-NOx ammonia combustor for a micro gas turbine. Proc Combust Inst 2019;37:4597–606.
[24] Gupta AK, Gupta AK, Lilley DG, Syred N. Tunbridge wells: tunbridge wells. In: Swirl flows. Abacus; 1984.
[25] Beer JMCNA. Combustion aerodynamics. London: Applied Science Publishers; 1972.
[26] Lefebvre AH. Gas turbine combustion/Arthur H. Lefebvre. Washington: Washington: Hemisphere Pub. Corp. : McGraw-Hill; 1983.
[27] Syred N, Beér JM. Combustion in swirling flows: a review. Combust Flame 1974;23:143–201.
[28] Hayakawa A, Arakawa Y, Mimoto R, Somarathne KDKA, Kudo T, Kobayashi H. Experimental investigation of stabilization and emission characteristics of ammonia/air premixed flames in a swirl combustor. Int J Hydrogen Energy 2017;42:14010–8.
[29] Cavaliere DE, Kariuki J, Mastorakos E. A comparison of the blow-off behaviour of swirl-stabilized premixed, non-premixed and spray flames. Flow, Turbul Combust 2013;91:347–72.
[30] Okafor EC, Somarathne KDKA, Ratthanan R, Hayakawa A, Kudo T, Kurata O, et al. Control of NOx and other emissions in micro gas turbine combustors fuelled with mixtures of methane and ammonia. Combust Flame 2020;211:406–16.
[31] Baukal CE, Eleazer PB. Quantifying NOx for industrial combustion processes. J Air Waste Manag Assoc 1998;48:52–8.
[32] Uk GOV. Monitoring stack emissions: guidance for selecting a monitoring approach. UK: GOV.; 2019.
[33] Gupta SK, Prabhudeva P, Kumar M, Ojha PK, Karmakar S. Investigation on spray combustion characteristics of Boron-Loaded slurry fuel in a Swirl-Stabilized combustor. Fuel 2022;323.
[34] Ma X, Wang Z, Jiang C, Jiang Y, Xu H, Wang J. An optical study of in-cylinder CH2O and OH chemiluminescence in flame-induced reaction front propagation using high speed imaging. Fuel 2014;134:603–10.
[35] Zhao M, Buttsworth D, Choudhury R. Experimental and numerical study of OH* chemiluminescence in hydrogen diffusion flames. Combust Flame 2018;197:369–77.
[36] Zhou S, Zhu X, Yan B, Gao Q, Chen G, Li B. Role of a hot coflow on establishment of MILD combustion of biomass gasified gas. Fuel 2022;314.
[37] Liu Y, Tan J, Wan M, Zhang L, Yao X. Quantitative measurement of OH* and CH* chemiluminescence in jet diffusion flames. ACS Omega 2020;5:15922–30.
[38] Pretzler G. A new method for numerical abel-inversion. Z Naturforsch 1991.
[39] Killer C. Abel inversion algorithm. MATLAB Central File Exchange; 2016.
[40] Runyon J, Marsh R, Bowen P, Pugh D, Giles A, Morris S. Lean methane flame stability in a premixed generic swirl burner: isothermal flow and atmospheric combustion characterization. Exp Therm Fluid Sci 2018;92:125–40.
[41] Okafor Ekenechukwu C, Sakai K, Hayakawa A, Kudo T, Kurata O, Iki N, et al. Stabilization and emission characteristics of ammonia flames in a micro gas turbine combustor. In: 11th asia-pacific conference on combustion; 2017. Australia.
[42] Choubey G, Tiwari M. Chapter Three - factors affecting the scramjet performance. In: Choubey G, Tiwari M, editors. Scramjet combustion. Butterworth-Heinemann; 2022. p. 49–63.
[43] Zhang M, Wei X, Wang J, Huang Z, Tan H. The blow-off and transient characteristics of co-firing ammonia/methane fuels in a swirl combustor. Proc Combust Inst 2021;38:5181–90.
[44] Somarathne KDKA, Okafor E C, Hayakawa A, Kudo T, Kurata O, Iki N, et al. Emission characteristics of turbulent non-premixed ammonia/air and methane/air swirl flames through a rich-lean combustor under various wall thermal boundary conditions at high pressure. Combust Flame 2019;210:247–61.
[45] Okafor EC, Tsukamoto M, Hayakawa A, Somarathne KDKA, Kudo T, Tsujimura T, et al. Influence of wall heat loss on the emission characteristics of premixed ammonia-air swirling flames interacting with the combustor wall. Proc Combust Inst 2021;38:5139–46.
[46] Zhang J, Sui C, Zhang B, Li J. Effects of swirl intensity on flame stability and NO emission in swirl-stabilized ammonia/methane combustion. Applications in Energy and Combustion Science 2023;14.